International Journal of Multiphase Flow 36 (2010) 449–459

Contents lists available at ScienceDirect

International Journal of Multiphase Flow

journal homepage: www.elsevier.com/locate/ijmulflow

Instability in gravity-driven flow over uneven permeable surfaces

J.P. Pascal [a,*], S.J.D. D'Alessio [b]

[a] Department of Mathematics, Ryerson University, Toronto, Ontario, Canada M5B 2K3
[b] Department of Applied Mathematics, University of Waterloo, Waterloo, Ontario, Canada N2L 3G1

ARTICLE INFO

Article history:
Received 9 August 2009
Received in revised form 5 March 2010
Accepted 10 March 2010
Available online 15 March 2010

Keywords:
Flow down an incline
Bottom topography
Linear and nonlinear stability analysis
Fluid–porous medium interface

ABSTRACT

We develop a theoretical model for inclined free-surface flow over a porous surface exhibiting periodic undulations. The effect of bottom permeability is incorporated by imposing a slip condition that accounts for the nonplanar geometry of the fluid–porous medium interface. Under the assumption of shallow flow, equations of motion accounting for inertial effects are obtained by retaining in the Navier-Stokes equations terms that are up to second-order with respect to a small shallowness parameter. The explicit dependence on the cross-stream coordinate is eliminated from these equations by means of a weighted residual procedure. A linear stability analysis of the steady flow is performed in connection with Floquet–Bloch theory. The results predict that bottom permeability has a destabilizing influence on the flow. A physical explanation has been proposed which involves examining how permeability affects the steady-state flow. Conclusions are drawn regarding the combined effect of the surface tension of the fluid and the parameters describing the bottom surface including permeability, inclination and the amplitude and wavelength of the undulations that generate the bottom topography. A numerical scheme for solving the fully nonlinear governing equations is also outlined. The instability of particular steady flows is determined by conducting nonlinear simulations of the temporal evolution of the flow and comparisons are made with the predictions from the linear analysis. Comparisons with existing experimental data are also included.

1. Introduction

Interfacial instabilities exhibited by inclined film flows have important consequences in many industrial processes. In certain cases the emergence of interfacial instability is an undesirable occurrence. In coating applications, for example, interfacial instability can cause an uneven distribution of material. In other industrial sectors film flows exhibiting large amplitude wave structures on the surface can optimize the process. Mass and heat exchangers, for example, operate more efficiently if the area of the liquid–gas interface which facilitates the transport is increased.

The critical conditions for the onset of instability in inclined flows and the development of the unstable flow are influenced by the structure of the solid surface at the bottom of the fluid layer. A theoretical investigation that incorporates such bottom effects as topography and permeability offers a more accurate flow model and can provide information on constructing surfaces that will induce the desired flow behaviour. In film flow applications these bottom effects are introduced by substrates with uneven surfaces composed of a porous material.

A thorough review of research on the various types of film flow has recently been compiled by Craster and Matar (2009). Contained in this paper is a survey of previous investigations of gravity-driven film flow including those which, like the present work, deal with flows involving significant inertial contributions, as well as those which neglect the effect of inertia and focus on the instability of contact lines which leads to the formation of the "fingering" phenomenon. Below we give specific mention to previous studies on gravity-driven flow which consider bottom topography and those which investigate the effect of bottom permeability.

Lately, several investigations have reported on gravity-driven flow over uneven, yet impermeable surfaces. The bottom topography is described by periodic undulations parameterized by measures of amplitude and wavelength. Wang (1981) studied steady creeping flow by employing an asymptotic analysis for small amplitudes of the bottom undulations. Pozrikidis (1988) also considered steady flows with negligible inertia and obtained numerical simulations for flow over corrugations with finite amplitude. Bontozoglou and Papapolymerou (1997) take into account inertial effects and carry out a linear analysis of steady flow under the assumption of small amplitude of the bottom undulations. Nonlinear effects and finite-amplitude bottom corrugations were considered by Trifonov (1998) for vertical flows, while Heining et al. (2009) dealt with arbitrary inclination. Trifonov (2007a) considered time-dependent flow down an uneven vertical surface and used a spectral method to carry

* Corresponding author.
E-mail addresses: jpascal@ryerson.ca (J.P. Pascal), sdalessio@uwaterloo.ca (S.J.D. D'Alessio).

0301-9322/$ - see front matter © 2010 Elsevier Ltd. All rights reserved.
doi:10.1016/j.ijmultiphaseflow.2010.03.003

out a linear stability analysis of the Navier-Stokes equations. In another investigation Trifonov (2007b) used the integrated-boundary-layer (IBL) approach proposed by Shkadov (1967) to study nonlinear effects in flows down vertical uneven surfaces. A Benney-type equation (Benney, 1966) for such flows was set up by Davalos-Orozco (2007). Recently, Oron and Heining (2008), also concentrating on the vertical flow case, implemented a mathematical model for flow over uneven topography based on the first-order weighted residual method proposed by Ruyer-Quil and Manneville (2000).

Flow over undulating surfaces with arbitrary inclination was considered by Tougou (1978) who proposed a Kuromoto–Sivashinsky type equation to describe the flow. However, the analysis did not capture the effect of bottom topography on the onset of instability. Wierschem et al. (2005) also investigated the flow along a wavy surface of arbitrary inclination. They performed a linear stability analysis using the shallow-flow approximations of the Navier-Stokes equations under assumptions of long bottom undulations, weak surface tension and Reynolds numbers of order unity. The results are confirmed by experimental findings and indicate that bottom topography has a stabilizing effect on the steady flow. The same general conclusion was reported by Vlachogiannis and Bontozoglou (2002) from their experiments of flows over corrugated surfaces. A stability analysis of shallow flow along an uneven surface of small, yet arbitrary inclination has been reported by Balmforth and Mandre (2004). Their model relies on the internal dissipation term proposed by Needham and Merkin (1984) for the shallow-water equations which cannot be coupled with the effects of the bottom configuration. Recently, D'Alessio et al. (2009) have implemented a second-order model for flows over uneven surfaces with moderate to steep inclination based on the weighted-residual method of Ruyer-Quil and Manneville (2000). This model incorporates important diffusive terms that are of second-order with respect to the shallowness of the flow, and in the even-bottom case is proven to correctly predict the critical conditions for the onset of flow instability, while accurately describing unstable flows as demonstrated in Ruyer-Quil and Manneville (2002).

The stability of flow along an incline with an even surface composed of a porous material was examined by Pascal (1999). Under an assumption of small permeability, the Orr-Sommerfeld equation was used in connection with a linear stability analysis to obtain critical conditions for the onset of instability. In Pascal (2006) a nonlinear analysis was carried out using the IBL equations. Recently, Thiele et al. (2009) considered flow over a porous surface without the restriction of small permeability, however their analytical investigation is limited to a linear stability analysis of a first-order Benney-type equation.

To the best of our knowledge the stability of flow over a permeable inclined surface exhibiting periodic undulations has not yet been studied. In the present work we undertake such an investigation by extending the model developed in D'Alessio et al. (2009) to account for bottom permeability with the aim of exploring the combined effect of bottom unevenness and permeability on the instability of the flow. The paper is organized as follows. In Section 2 we describe how the effect of bottom permeability is incorporated into the equations of motion for the fluid layer and we establish the depth-integrated flow model. In Section 3 a linear stability analysis is performed, while in Section 4 a numerical method is presented for solving the fully nonlinear governing equations and obtaining the entire evolution of a perturbed equilibrium flow. The predictions for the onset of instability made by these calculations are compared with those from the linear analysis, and the solution for the surface profile is used to investigate the interfacial wave pattern associated with flow instability. Lastly, a summary is included in the concluding section. Two appendices, Appendices A and B, are also included to present details surrounding the Benney equation and the numerical solution procedure, respectively.

2. Governing equations

We consider the two-dimensional laminar flow of a shallow layer of a Newtonian fluid with no external forcing at the surface along an uneven inclined surface as shown in Fig. 1. We define an (x,z) coordinate system with the x-axis inclined at an angle θ with respect to the horizontal and pointing in the downhill direction, and with the z-axis pointing in the upward normal direction. The inclined solid over which the fluid is flowing is assumed to be porous and saturated with fluid and assumed to have periodic undulations on its surface expressed by

$$z = \zeta(x) = A_b \cos\left(\frac{2\pi x}{\lambda_b}\right),$$

with the parameters A_b and λ_b characterizing the amplitude and wavelength of the undulations, respectively. The fluid velocity is denoted by $\mathbf{u} = (u,w)^T$.

In scaling the equations of motion, for the vertical length scale we employ the Nusselt thickness of flow along an impermeable surface resulting from a constant discharge, Q, which is given by

$$H = \left(\frac{3\mu Q}{\rho g \sin\theta}\right)^{1/3},$$

where g is the acceleration due to gravity and ρ, μ are the fluid density and viscosity, respectively. Another evident possibility for the vertical length scale is the Nusselt thickness corresponding to flow along a permeable surface. However, the previously mentioned scale is preferable since it allows for the permeability of the bottom surface to be introduced into our model as an independent parameter.

The pressure is scaled using ρU^2 where $U = Q/H$ is the velocity scale. The corresponding time scale is taken to be l/U where l is the horizontal length scale. An obvious choice for the horizontal length scale is $l = \lambda_b$. As the shallowness parameter we select $\delta = H/l = H/\lambda_b$. The scaled bottom profile is then given by

$$\zeta(x) = a_b \cos(2\pi x) \text{ where } a_b = \frac{A_b}{H} = \frac{1}{\delta}\frac{A_b}{\lambda_b}.$$

In this study we will consider small bottom waviness having $A_b/\lambda_b = O(\delta)$ and thus $a_b = O(1)$.

The equations of motion in the fluid layer and the conditions at the surface are identical to those corresponding to the impermeable bottom case. As detailed in D'Alessio et al. (2009) these equations are obtained from the two-dimensional Navier-Stokes equations by assuming the Reynolds number, $\mathrm{Re} = \rho Q/\mu$, to be $O(1)$ and neglecting terms which are $O(\delta^3)$. The continuity equation is given by

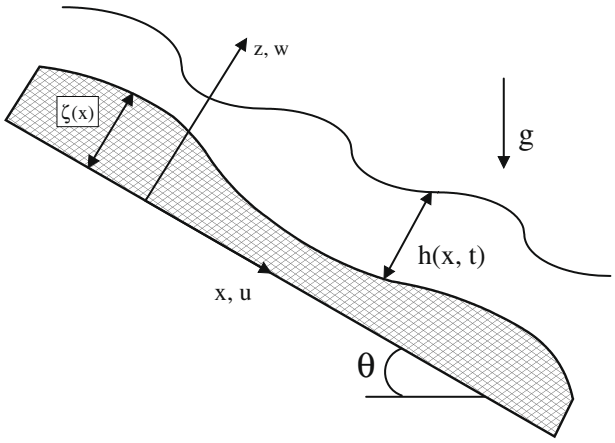

Fig. 1. The flow configuration.

$$\frac{\partial u}{\partial x}+\frac{\partial w}{\partial z}=0, \tag{1}$$

while using the z-momentum equation to eliminate the pressure from the x-momentum yields:

$$\delta \mathrm{Re}\frac{Du}{Dt}=-3\cot\theta\delta\frac{\partial z_1}{\partial x}+\delta^2\frac{\partial}{\partial x}\left(\left.\frac{\partial u}{\partial x}\right|_{z=z_1}\right)+\delta^2\frac{\partial^2 u}{\partial x^2}+\mathrm{Re}\delta^3 S\frac{\partial^3 z_1}{\partial x^3}+3+\delta^2\frac{\partial^2 u}{\partial x^2}+\frac{\partial^2 u}{\partial z^2}. \tag{2}$$

In this equation $\frac{D}{Dt}$ denotes the two-dimensional material derivative, $z_1=\zeta(x)+h(x,t)$ is the free surface and $S=TH/(\rho Q^2)$, with T referring to the surface tension of the fluid. The surface tension parameter S can be interpreted as an inverse Weber number and is assumed to be of order $1/\delta^2$ or larger.

At the surface of the fluid layer we have the tangential force condition

$$\frac{\partial u}{\partial z}-4\delta^2\frac{\partial z_1}{\partial x}\frac{\partial u}{\partial x}+\delta^2\frac{\partial w}{\partial x}=0 \text{ at } z=z_1, \tag{3}$$

together with the kinematic condition expressed as

$$w=\frac{\partial h}{\partial t}+u\frac{\partial h}{\partial x}+u\zeta'(x) \text{ at } z=z_1. \tag{4}$$

In order to incorporate the effect of the permeability of the bottom and the filtration flow through it we impose a slip-velocity condition at the fluid–porous medium interface. Such a condition was originally proposed by Beavers and Joseph (1967) in connection with their investigation of Stokes flow over a porous medium the flow through which is assumed to be governed by Darcy's law. The Beavers and Joseph condition has been employed by several researchers in connection with stability analysis of flows over porous surfaces being governed by the Navier-Stokes equations. The Poiseuille flow over porous surfaces has been recently investigated by Chang et al. (2006) and Liu et al. (2008), while the gravity-driven flow with a free surface was considered by Davis and Hocking (1999), Pascal (1999), Miglio et al. (2003), Pascal (2006), and Sadiq and Usha (2008).

Saffman (1971) gave a theoretical justification of the Beavers and Joseph condition and presented a formulation suitable for the general nonplanar geometry expressed as

$$\frac{\partial v^{\parallel}}{\partial \mathbf{N}}=\frac{\alpha}{\sqrt{\kappa}}\left(v^{\parallel}-v_p^{\parallel}\right),$$

where $v^{\parallel}$ is the component of the dimensional velocity of the fluid that is tangent to the interface, $\mathbf{N}$ is the normal unit vector to the interface pointing into the fluid and $v_p^{\parallel}$ is the tangential component of the mean filtration velocity in the porous medium. The permeability of the porous medium is denoted by κ and α is a dimensionless empirical parameter which is found to depend on the structure of the porous medium. Scaling this condition while using $\frac{\kappa\rho g\sin\theta}{\mu}$ as the scale for the filtration velocity we obtain:

$$\frac{\delta_1}{\left[1+\delta^2(\zeta')^2\right]^{3/2}}\left\{\left[\frac{\partial u}{\partial z}+\delta^2\zeta'\frac{\partial w}{\partial z}-\delta^2\zeta'\frac{\partial u}{\partial x}-\delta^4\zeta'\zeta''w-\delta^4(\zeta')^2\frac{\partial w}{\partial x}\right]\left[1+\delta^2(\zeta')^2\right]+\delta^4(\zeta')^2\zeta''(u+\delta^2\zeta' w)\right\}=u+\delta^2\zeta' w-\delta^3(u_p+\delta^2\zeta' w_p) \text{ at } z=\zeta(x),$$

where u_p and w_p are the dimensionless filtration velocity components in the porous medium and δ_1 is a permeability parameter given by

$$\delta_1=\frac{\sqrt{\kappa}}{\alpha H}.$$

Continuity of the normal velocity component at the fluid–porous medium interface is expressed as:

$$w-\zeta' u=\delta^3(w_p-\zeta' u_p) \text{ at } z=\zeta(x).$$

In the present study we assume that $\delta_1=O(\delta)$. Considering that in the experiments of Beavers and Joseph the parameter α varies between 0.1 and 0.4, our assumption is consistent with Darcy numbers, $Da=\frac{\kappa}{H^2}$, ranging from 10^{-4} to 10^{-2}. This range includes circumstances considered in experimental investigations and occurring in flows over natural surfaces and substrates involved in industrial processes. Neglecting terms of order δ^3 and higher in the two conditions at the interface listed above we obtain:

$$\delta_1\frac{\partial u}{\partial z}=u+\delta^2\zeta' w \text{ at } z=\zeta(x), \tag{5}$$

and

$$w=\zeta' u \text{ at } z=\zeta(x). \tag{6}$$

A variant of the Beavers and Joseph condition was proposed by Jones (1973) who stipulated that the velocity gradient should be replaced by shear stress. Extending the Jones condition to the case of a nonplanar interface we obtain

$$(\dot{\gamma}\mathbf{N})\cdot\mathbf{T}=\frac{\alpha}{\sqrt{\kappa}}\left(v^{\parallel}-v_p^{\parallel}\right),$$

where $\dot{\gamma}$ is the shear rate tensor and $\mathbf{T}$ is the unit vector tangent to the interface. We find however that to $O(\delta^3)$ the Jones condition coincides with the Saffman condition given by Eq. (5).

In using Eqs. (1)–(6) to describe the flow, the effect of bottom permeability is incorporated through the slip condition at the interface given by Eq. (5), but the flow is decoupled from the filtration flow in the porous medium. Thiele et al. (2009) took into account the filtration flow in establishing a Benney-type equation for the thickness of a fluid layer flowing down an even porous incline. However, they discovered that for small permeability the results are in good agreement with those from the equation obtained if the effect of the porous medium is solely included by means of a slip condition at the fluid–porous medium interface.

We proceed by depth integrating the equations of motion with the aim of eliminating the cross-flow variation. This course of action is justified by the assumed shallowness of the fluid layer and the expectation of a flow which varies slowly in the longitudinal direction. Depth integrating the continuity Eq. (1) and incorporating the kinematic condition (4) yields

$$\frac{\partial h}{\partial t}+\frac{\partial q}{\partial x}=0, \tag{7}$$

where the flow rate, q, is given by

$$q=\int_{\zeta(x)}^{\zeta(x)+h}u\,dz.$$

The depth integration of the momentum Eq. (2) can be accomplished by applying a weighted residual method based on the expansion of the longitudinal velocity. In exploring flows over impermeable and even inclines this approach was originally implemented by Ruyer-Quil and Manneville (2000). They considered an expansion of the longitudinal velocity of the form $u=\sum_{j=0}^{J}a_j(x,t)\,b_j(z)$, where for $0\leqslant j\leqslant J$, $b_j(z)$ are polynomial test functions and $a_j(x,t)$ are their amplitudes, with $b_0(z)$ being taken to be the semi-parabolic profile of the Nusselt flow. Resulting from the fact that the test functions are polynomials, it turns out that only three terms need to be taken in this expansion, and partial differential equations governing the amplitude functions are obtained using a weighted residual method.

Ruyer-Quil and Manneville demonstrate that the amplitudes a_j with $j\geqslant 1$ have much shorter relaxation times than that of a_0 and thus argue that the adiabatic elimination of these functions is warranted. Based on this assumption they obtain a simpler set of governing equations involving q and h which we will refer to as the

second-order modified IBL equations. In Ruyer-Quil and Manneville (2002) the authors consider several different weighted residual methods in connection with the adiabatic elimination approximation whereby the derivatives of a_j with $j \geqslant 1$ are assumed to be negligible. They found that for all the methods considered the equations ultimately converged to the modified IBL equations as more terms were retained in the series. However, the Galerkin method is optimal since convergence is reached with only one term in the expansion. Scheid et al. (2006) used a Padé approximant to obtain a refined version of the modified IBL equations which is able to capture the occurrence of a counter flow at the front of solitary waves on flows along even and impermeable inclines as predicted by the direct numerical simulations carried out by Malamataris et al. (2002). This approach is not followed in the present investigation due to the complications resulting from the assumed bottom unevenness and permeability.

The important advantage that the modified IBL equations have over the original IBL equations is that their prediction for the onset of flow instability is in exact agreement with that from the Orr-Sommerfeld equations as reported in Benjamin (1957) and Yih (1963), which has itself been experimentally verified by Liu et al. (1993). The modified IBL equations also offer an important advantage over the Benney equation as they are able to capture the nonlinear development of supercritical flows as demonstrated by Ruyer-Quil and Manneville (2002) who compare the results with the experimental observations reported by Liu et al. (1995) and the direct numerical simulations carried out by Ramaswamy et al. (1996).

For the present problem of flow over an undulating permeable substrate the one term velocity expansion to be used in connection with the Galerkin method is

$$u = \frac{3q}{2\left(h^3 + 3\delta_1 h^2\right)} b_0,$$

where b_0 is given by

$$b_0 = 2(h + \zeta(x))z - z^2 - \zeta(x)^2 - 2\zeta(x)h + 2\delta_1 h.$$

Following the Galerkin approach and utilizing b_0 as the weight function, we multiply Eq. (2) by b_0 and integrate with respect to z from $\zeta(x)$ to $h + \zeta(x)$ to obtain the following dimensionless equations for the flow variables h and q:

$$\frac{\partial h}{\partial t} + \frac{\partial q}{\partial x} = 0, \tag{8}$$

$$\begin{aligned}
&\left(\delta + 2\frac{\delta\delta_1}{h}\right)\frac{\partial q}{\partial t} - \left(\frac{5}{6}h\frac{d^3\zeta}{dx^3} + \frac{5}{6}h\frac{\partial^3 h}{\partial x^3} + \frac{5}{2}\delta_1\frac{d^3\zeta}{dx^3} + \frac{5}{2}\delta_1\frac{\partial^3 h}{\partial x^3}\right)S\delta^3 \\
&- \left(-5\frac{q\left(\frac{d\zeta}{dx}\right)^2}{h^2\mathrm{Re}} + \frac{9}{2}\frac{\frac{\partial^2 q}{\partial x^2}}{\mathrm{Re}} - \frac{5}{2}\frac{q\left(\frac{\partial h}{\partial x}\right)\frac{d\zeta}{dx}}{h^2\mathrm{Re}} - 6\frac{q\frac{\partial^2 h}{\partial x^2}}{h\mathrm{Re}} - \frac{15}{4}\frac{q\frac{d^2\zeta}{dx^2}}{h\mathrm{Re}}\right. \\
&\left. + 4\frac{q\left(\frac{\partial h}{\partial x}\right)^2}{h^2\mathrm{Re}} - \frac{9}{2}\frac{\left(\frac{\partial q}{\partial x}\right)\frac{\partial h}{\partial x}}{h\mathrm{Re}}\right)\delta^2 - \left(\frac{9}{7}\frac{q^2\frac{\partial h}{\partial x}}{h^2} - \frac{5}{2}\frac{h\cot\theta\frac{\partial h}{\partial x}}{\mathrm{Re}} - \frac{5}{2}\frac{h\cot\theta\frac{d\zeta}{dx}}{\mathrm{Re}}\right. \\
&\left. - \frac{17}{7}\frac{\left(\frac{\partial q}{\partial x}\right)q}{h} - \frac{17}{7}\frac{\delta_1\left(\frac{\partial q}{\partial x}\right)q}{h^2}\right)\delta + \left(\frac{15}{2}\frac{\cot\theta\frac{d\zeta}{dx}}{\mathrm{Re}} + \frac{45}{16}\frac{q^2\frac{d\zeta}{dx}}{h^3} + \frac{15}{2}\frac{\cot\theta\frac{\partial h}{\partial x}}{\mathrm{Re}}\right)\delta_1\delta \\
&+ \frac{5}{2}\frac{q}{h^2\mathrm{Re}} - \frac{5}{2}\frac{h}{\mathrm{Re}} - \frac{15}{2}\frac{\delta_1}{\mathrm{Re}} = 0.
\end{aligned} \tag{9}$$

In the impermeable bottom case, which is obtained by setting $\delta_1 = 0$, these equations reduce to those obtained in D'Alessio et al. (2009) which in turn coincide with the second-order modified IBL equations obtained by Ruyer-Quil and Manneville in the even-bottom case which corresponds to setting $\zeta(x) \equiv 0$.

3. Linear stability analysis

From Eq. (8) we obtain that the steady-state solution for q is a constant. If we use this constant as the discharge scale Q, then in dimensionless form we have that $q = q_s = 1$ and $h = h_s(x)$ where $h_s(x)$ satisfies the nonlinear differential equation given by

$$\begin{aligned}
&\frac{5}{6}\delta^2 S(h_s + 3\delta_1)h_s^2 h_s''' - \frac{2\delta}{\mathrm{Re}}[3h_s h_s'' - 2(h_s')^2] \\
&- \left(\frac{5\cot\theta}{2\mathrm{Re}}h_s^3 + \frac{5\delta}{2\mathrm{Re}}\zeta' + \frac{15\delta_1\cot\theta}{2\mathrm{Re}}h_s^2 - \frac{9}{7}\right)h_s' \\
&- \frac{15\delta}{4\mathrm{Re}}\zeta''' h_s + \left(\frac{5}{2\delta\mathrm{Re}} - \frac{5\cot\theta}{2\mathrm{Re}}\zeta' + \frac{5}{6}\delta^2 S\zeta'''\right)(h_s + 3\delta_1)h_s^2 \\
&- \frac{45\delta_1}{16}\frac{\zeta'}{h_s} = \frac{5}{2\delta\mathrm{Re}} + \frac{5\delta}{\mathrm{Re}}(\zeta')^2,
\end{aligned} \tag{10}$$

with the prime denoting differentiation with respect to x and once again $\zeta(x) = a_b\cos(2\pi x)$.

To study how small disturbances will evolve when superimposed on the steady equilibrium solution, we linearize the governing equations by introducing perturbations $\hat{h}, \hat{q}$ and set

$$h = h_s(x) + \hat{h}, \quad q = 1 + \hat{q}.$$

The linearized perturbation equations can then be written in the form

$$\frac{\partial\hat{h}}{\partial t} + \frac{\partial\hat{q}}{\partial x} = 0, \tag{11}$$

$$\begin{aligned}
&\frac{\partial\hat{q}}{\partial t} - \frac{9\delta h_s}{2\mathrm{Re}(h_s + 2\delta_1)}\frac{\partial^2\hat{q}}{\partial x^2} + f_1\frac{\partial\hat{q}}{\partial x} + f_2\hat{q} + f_3\hat{h} + f_4\frac{\partial\hat{h}}{\partial x} \\
&\quad + \frac{6\delta}{\mathrm{Re}(h_s + 2\delta_1)}\frac{\partial^2\hat{h}}{\partial x^2} + f_5\frac{\partial^3\hat{h}}{\partial x^3} = 0,
\end{aligned} \tag{12}$$

where

$$f_1(x) = \frac{34\mathrm{Re}h_s + 63\delta h_s h_s' + 34\delta_1\mathrm{Re}}{14\mathrm{Re}(h_s + 2\delta_1)h_s},$$

$$\begin{aligned}
f_2(x) = \frac{1}{56\mathrm{Re}\delta(h_s + 2\delta_1)h_s^2}&\left(140h_s - 224\delta^2 h_s(h_s')^2 + 336\delta^2 h_s^2 h_s''\right. \\
&- 144\delta\mathrm{Re}h_s h_s' + 210\delta^2\zeta'' h_s^2 + 140\delta^2\zeta' h_s h_s' + 280\delta^2(\zeta')^2 h_s \\
&\left. + 315\delta\delta_1\mathrm{Re}\zeta'\right),
\end{aligned}$$

$$\begin{aligned}
f_3(x) = \frac{1}{336\mathrm{Re}\delta(h_s + 2\delta_1)h_s^3}&\left(-2016\delta^2 h_s^2 h_s'' + 840\delta\cot\theta\zeta' h_s^4\right. \\
&+ 864\mathrm{Re}\delta h_s h_s' - 1680h_s - 280\delta^3 S\mathrm{Re}h_s^4 h_s''' \\
&- 840h_s^4 - 3360\delta^2(\zeta')^2 h_s + 2688\delta^2 h_s(h_s')^2 - 1680\delta^2 h_s h_s'\zeta' \\
&\left. - 2835\delta\delta_1\mathrm{Re}\zeta' - 280\delta^3 S\mathrm{Re}h_s^4\zeta''' - 1260\delta^2\zeta'' h_s^2 + 840\delta\cot\theta h_s^4 h_s'\right),
\end{aligned}$$

$$f_4(x) = \frac{-112\delta h_s' - 18\mathrm{Re} + 35\delta\zeta' + 35\cot\theta h_s^3 + 105\cot\theta\delta_1 h_s^2}{14\mathrm{Re}h_s(h_s + 2\delta_1)},$$

$$f_5(x) = \frac{-5\delta^2 S h_s(h_s + 3\delta_1)}{6(h_s + 2\delta_1)}.$$

(13)

We first entertain the case of an even bottom having $\zeta(x) \equiv 0$. In this case Eq. (10) admits a constant solution, h_0, satisfying the algebraic equation

$$h_0^3 + 3\delta_1 h_0^2 - 1 = 0.$$

The exact solution of this equation is obtainable, however here we present only the asymptotic expansion of the solution for small δ_1 up to $O(\delta_1^3)$:

$$h_0 = 1 - \delta_1 + \delta_1^2 + O(\delta_1^3).$$

For the even bottom case the linearized perturbation equations have constant coefficients and we accordingly introduce normal modes of the form

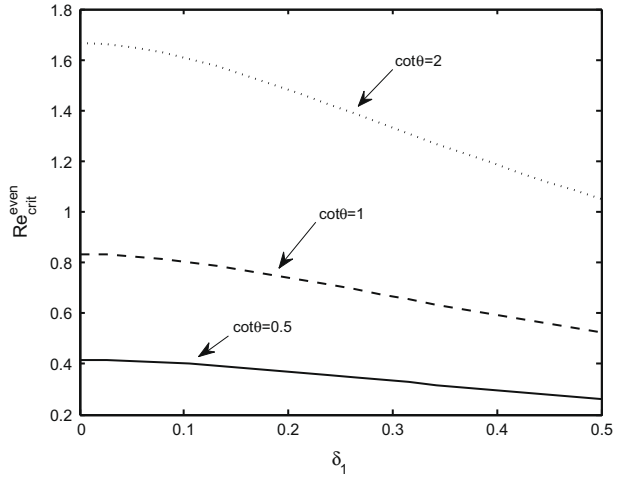

Fig. 2. The critical Reynolds number for the even bottom case.

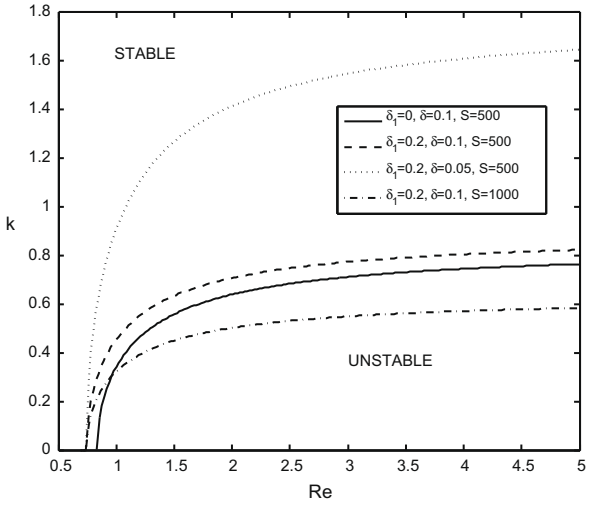

Fig. 3. Neutral stability curves for the even bottom case with $\cot\theta = 1$.

$\hat{h} = \tilde{h}e^{\sigma t}e^{ikx}$ and $\hat{q} = \tilde{q}e^{\sigma t}e^{ikx}$.

The associated dispersion relation is given by

$$\left(42\delta h_0^3\mathrm{Re} + 84\delta h_0^2\mathrm{Re}\delta_1\right)\sigma^2 + \left(105h_0 + 102i\delta h_0^2 k\mathrm{Re} + 102i\delta h_0\delta_1 k\mathrm{Re} + 189\delta^2 h_0^3 k^2\right)\sigma + 210ik + 105ikh_0^3 + 35Sk^4\delta^3 h_0^4\mathrm{Re} + 105Sk^4\delta^3 h_0^3\mathrm{Re}\delta_1 + 252i\delta^2 h_0^2 k^3 - 54\delta h_0 k^2\mathrm{Re} + 105\delta h_0^4\cot\theta k^2 + 315\delta h_0^3\cot\theta\delta_1 k^2 = 0.$$

Analyzing this equation we find that there is a critical Reynolds number $\mathrm{Re}_{crit}^{even}$ such that if $\mathrm{Re} \leqslant \mathrm{Re}_{crit}^{even}$ then the real part of σ is non-positive for perturbations of any wavenumber k, while if $\mathrm{Re} > \mathrm{Re}_{crit}^{even}$ then there exists a critical wavenumber k_{max} such that the real part of σ is positive if and only if $k < k_{max}$. Consequently, $\mathrm{Re}_{crit}^{even}$ is the critical Reynolds number for flow instability, and for supercritical flows only perturbations that are sufficiently long become unstable.

Exact analytic solutions for $\mathrm{Re}_{crit}^{even}$ and k_{max} have been obtained but the expressions are very long and elaborate and explicitly presenting them here would serve little purpose. We can say that upon inspecting these expressions it can readily be seen that while k_{max} is dependent on all the parameters, $\mathrm{Re}_{crit}^{even}$ only varies with $\cot\theta$ and δ_1, i.e. the critical Reynolds number for the onset of flow instability is only dependent on the inclination and permeability of the bottom surface. In Fig. 2 we present the dependence of $\mathrm{Re}_{crit}^{even}$ on δ_1 for several bottom inclinations. The indication is that bottom permeability acts to destabilize the flow. An explanation of this effect will be outlined later in this section. In Fig. 3 we use the solution for k_{max} to obtain several neutral stability curves in the $\mathrm{Re} - k$ plane. Up to $O(\delta_1^3)$ the solution for $\mathrm{Re}_{crit}^{even}$ is given by

$$\mathrm{Re}_{crit}^{even} = \frac{5}{6}\cot\theta\left(1 - \frac{29}{7}\delta_1^2\right) + O(\delta_1^3).$$

When the difference in scaling is taken into account, this result is in agreement with that predicted by the Orr-Sommerfeld equation as obtained by Pascal (1999). Also, with $\delta_1 = 0$ the expression for $\mathrm{Re}_{crit}^{even}$ reduces to $\frac{5}{6}\cot\theta$ which is the well-known result for flow over impermeable surfaces. An alternate stability analysis employing the first-order Benney equation is presented in Appendix A which yields a result that comes in close agreement to that above.

For the case of an uneven bottom, the coefficients in Eq. (12) are periodic functions. We thus apply Floquet–Bloch theory to conduct the stability analysis. Consequently, we represent the perturbations as Bloch-type functions having the form

$$\hat{h} = e^{\sigma t}e^{iKx}\sum_{n=-\infty}^{\infty}\hat{h}_n e^{i2\pi nx}, \quad \hat{q} = e^{\sigma t}e^{iKx}\sum_{n=-\infty}^{\infty}\hat{q}_n e^{i2\pi nx}.$$

The exponential factor containing the Bloch wavenumber, K, represents disturbances which interact with the periodic bottom topography via the equilibrium flow, which is represented by the Fourier series composed of its harmonics. Introducing the Bloch-type functions with truncated series into the perturbation equations yields an algebraic eigenvalue problem. This problem can be solved numerically for the temporal growth rate given by the real part of σ. In this way we can determine the critical Reynolds number for the onset of instability, and for supercritical flows we can compute the wavelength and speed of unstable disturbances.

In Fig. 4 we display the variation of the critical Reynolds number, Re_{crit}, with the amplitude of the bottom undulations, a_b, for several values of the surface tension parameter, S. An evident consequence of bottom topography is to introduce a dependence of Re_{crit} on S. In other words, surface tension influences the onset of instability for flows over uneven surfaces.

In Figs. 5 and 6 we display the variation with S of $\mathrm{Re}_{crit}^{even} - \mathrm{Re}_{crit}$, the difference in the critical Reynolds numbers corresponding to the cases with and without bottom topography. Negative values

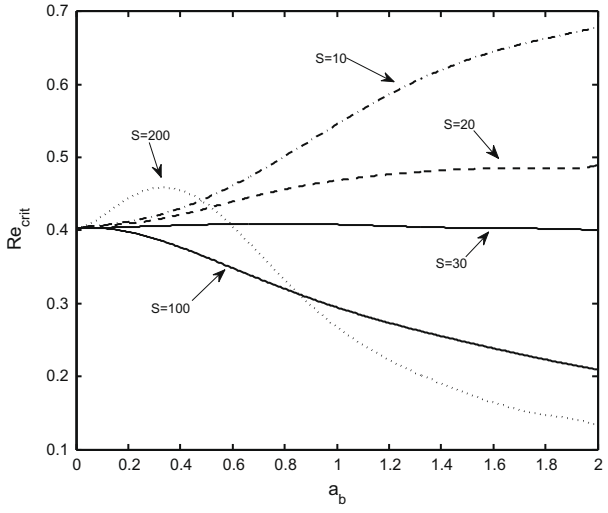

Fig. 4. Critical Reynolds number as a function of bottom amplitude with $\cot\theta = 0.5$, $\delta = 0.1$ and $\delta_1 = 0.1$.

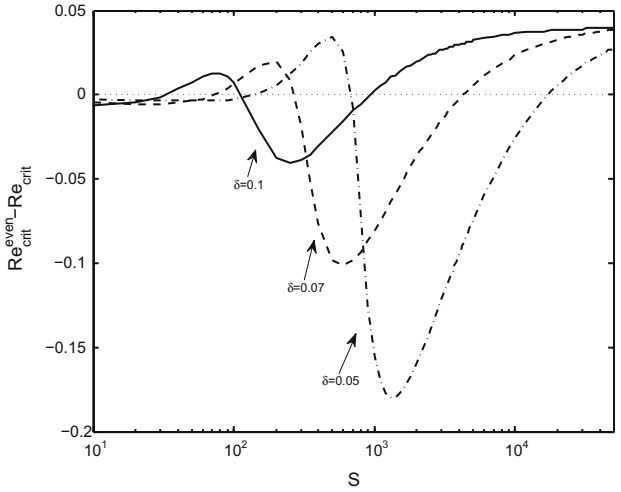

Fig. 5. Critical Reynolds number difference as a function of S with $a_b = 0.2$, $\delta_1 = 0.1$ and $\cot\theta = 0.5$.

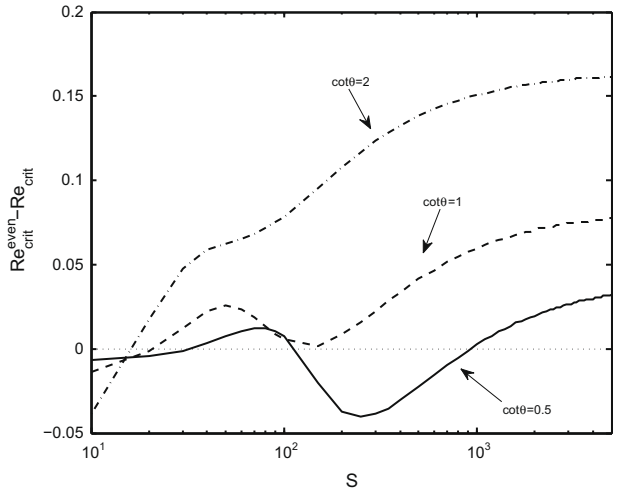

Fig. 6. Critical Reynolds number difference as a function of S with $a_b = 0.2$, $\delta_1 = 0.1$ and $\delta = 0.1$.

for this function then indicate that bottom topography acts to stabilize the flow, while positive values indicate that bottom topography has a destabilizing effect. Values of S where the function is zero correspond to "transition points" in the sense that as S is increased through these values the destabilizing role of bottom topography is reversed. The reversal in the stabilizing effect of bottom topography as S is increased was first discovered in D'Alessio et al. (2009) and subsequently confirmed by Heining and Aksel (2009) who conducted their investigation by considering the inverse problem. In the present work we now examine a broader range of surface tension values and find several transition points. In Fig. 5 we fix the bottom inclination at $\cot\theta = 0.5$ and include the difference variation for several values of δ. It can be seen that bottom topography acts to stabilize the flow with the exception of large S values and a compact interval of S values in the intermediate range. It is also apparent that as δ is decreased the curves become steeper at the second transition point. Based on our scaling, decreasing δ can be associated with increasing the wavelength of the bottom undulations.

In Fig. 6 we present the curves for the critical Reynolds number difference corresponding to various inclination values. We can conclude from these results that for gentle inclinations bottom unevenness destabilizes the flow for a wide range of S values with the stabilizing effect of bottom topography being limited to flows with weak surface tension. As the bottom inclination is increased, the stabilizing effect of bottom topography is encountered at an increasing range of S values, and for sufficiently steep inclination an undulating bottom only destabilizes the flow when combined with strong surface tension.

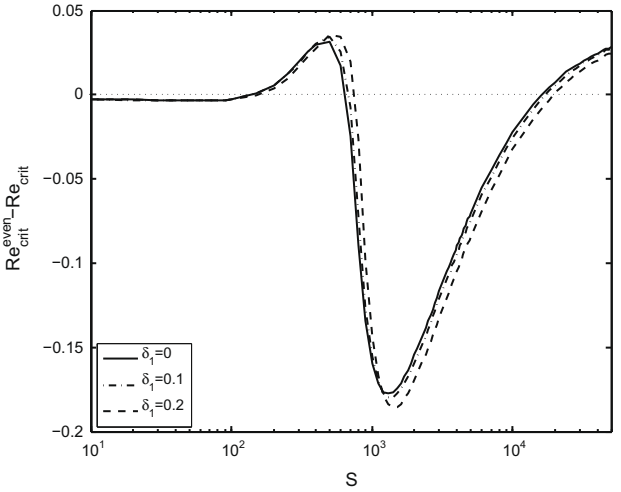

Fig. 7. Critical Reynolds number difference as a function of S with $a_b = 0.2$, $\delta = 0.05$ and $\cot\theta = 0.5$.

As discussed above, in spite of being restricted to a small range of values by the assumptions of our model, the parameter δ has an important effect on the results. We have discovered, on the other hand, that in most cases varying the permeability parameter, δ_1, has little impact on Re_{crit} and no qualitative inferences can be made about its impact with the exception of the anticipated conclusion that bottom permeability destabilizes the flow. In Fig. 7 we give the $Re^{even}_{crit} - Re_{crit}$ variation with S for different values of δ_1. It can be seen that for most S values the introduction of bottom permeability has little effect on Re_{crit} and has no impact on whether bottom topography stabilizes or destabilizes the flow. However, for an S value in the vicinity of the second zero of the difference function we expect that there is sufficient variation in Re_{crit} with δ_1 to have a notable impact on the stability of the flow. Indeed, the Re_{crit} as a function of a_b curves displayed in Fig. 8 reveal that for sufficiently large a_b bottom permeability effectuates a significant change in the critical Reynolds number and causes a reversal in the destabilizing role played by bottom unevenness.

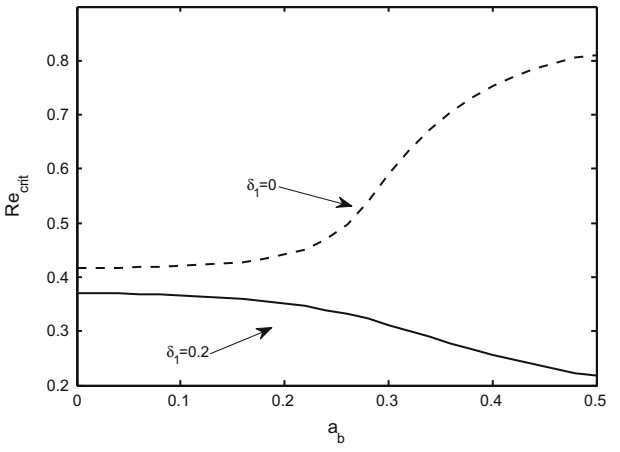

Fig. 8. Critical Reynolds number as a function of bottom amplitude with $\cot\theta = 0.5$, $\delta = 0.05$ and $S = 700$.

We have seen that bottom permeability destabilizes the flow for the even bottom case and Fig. 8 suggests that the same is true for an uneven bottom. An explanation as to why a porous surface destabilizes the flow will next be presented. This involves examining how permeability alters the steady-state solution and the interaction between bottom topography and permeability. We start by expanding the steady-state flow variables u_s, w_s, p_s in the following series

$$u_s(x,z) = u_0(x,z) + \delta u_1(x,z) + \delta^2 u_2(x,z) + \cdots,$$
$$w_s(x,z) = w_0(x,z) + \delta w_1(x,z) + \delta^2 w_2(x,z) + \cdots,$$
$$p_s(x,z) = p_0(x,z) + \delta p_1(x,z) + \delta^2 p_2(x,z) + \cdots.$$

These expansions are then substituted into the steady-state two-dimensional Navier-Stokes equations. Equating powers of δ results in a closed system of equations at each order. The same is done for the corresponding boundary conditions (5) and (6). The steady-state solution $h_s(x)$ can also be expanded in a series by resorting to Eq. (10). It can be easily shown that

$$h_s(x) = h_0 + \delta h_1(x) + O(\delta^2),$$

where the constant h_0 is identical to that for the even bottom case and

$$h_1(x) = \frac{1}{(h_0+2\delta_1)}\left(\frac{h_0(h_0+3\delta_1)\cot\theta}{3(h_0+2\delta_1)} + \frac{3\mathrm{Re}\delta_1}{8h_0^2}\right)\zeta'(x).$$

Although this procedure is similar to that used in deriving the Benney equation discussed in Appendix A, there are some significant differences. For example, the Benney equation represents an unsteady evolution equation for h which emanates from the kinematic condition, whereas in the approach developed here the kinematic condition is not used. For simplicity, we will consider the case of negligible surface tension.

The leading order problem is governed by the equations

$$\frac{\partial p_0}{\partial z} = -\frac{3\cot\theta}{\mathrm{Re}}, \quad \frac{\partial^2 u_0}{\partial z^2} = -3, \quad \frac{\partial w_0}{\partial z} = -\frac{\partial u_0}{\partial x},$$

and the following boundary conditions

$$\delta_1 = \frac{\partial u_0}{\partial z} = u_0, w_0 = \zeta u_0$$
$$p_0 = \frac{\partial u_0}{\partial z} = 0 \text{ at } z = h_0 + \zeta(x).$$

The solution to the leading order problem is given by

$$p_0(x,z) = \frac{3\cot\theta}{\mathrm{Re}}(h_0+\zeta-z),$$
$$u_0(x,z) = -\frac{3}{2}(z-\zeta)^2 + 3h_0(z-\zeta) + 3h_0\delta_1,$$
$$w_0(x,z) = -\frac{3}{2}\zeta'(z-\zeta)^2 + 3h_0\zeta'(z-\zeta) + 3h_0\delta_1\zeta'.$$

We note that although the kinematic condition was not imposed in arriving at the above solutions, $w_0(x,z)$ does, in fact, satisfy the free-surface condition $w_0(x, z = h_0+\zeta) = u_0(x, z = h_0+\zeta)\zeta'$. Continuing this procedure to second-order we obtained the approximate steady-state solution for u_s:

$$u_s(x,z) \approx u_0(x,z) + \delta u_1(x,z) + \delta^2 u_2(x,z)$$

where

$$u_1(x,z) = 3\cot\theta\zeta'\left(\frac{1}{2}(z-\zeta)^2 - h_0(z-\zeta) - h_0\delta_1\right),$$
$$u_2(x,z) = 3(\zeta')^2(z-\zeta)^2 + K(z-\zeta) + 6\zeta''\left(-\frac{1}{6}(z-\zeta)^3 + \frac{h_0}{2}(z-\zeta)^2\right)$$
$$+ 9\cot\theta\mathrm{Re}\zeta''\left(-\frac{1}{360}(z-\zeta)^6 + \frac{h_0}{60}(z-\zeta)^5 - \frac{h_0^2}{24}(z-\zeta)^4\right.$$
$$\left. - \frac{h_0^2\delta_1}{6}(z-\zeta)^3 - \frac{h_0^2\delta_1^2}{2}(z-\zeta)^2\right), + \delta_1 K - 3h_0(\zeta^1)^2\left(\delta_1 + \frac{h_0}{2}\right),$$

with

$$K(x) = -6h_0(\zeta')^2 - 3h_0\zeta''\left(\delta_1 + \frac{3h_0}{2}\right) + 9\cot\theta\mathrm{Re}\zeta''\left(\frac{h_0^5}{10} + \frac{h_0^4\delta_1}{2} + h_0^3\delta_1^2\right).$$

Equipped with this approximate solution for $u_s(x,z)$ we can next determine the steady flow rate, Q_s, by evaluating

$$Q_s(x) = \int_\zeta^{h_0+\zeta} u_s(x,z)dz,$$

and then compute the average value over the bottom topography to give $\overline{Q}_s$ where

$$\overline{Q}_s = \int_0^1 Q_s(x)dx.$$

Following this procedure we obtain

$$\overline{Q}_s(\delta_1) \approx 1 - 2\pi^2 a_b^2 h_0^2\left(\frac{7h_0}{2} + 9\delta_1\right)\delta^2.$$

To arrive at this expression we have made use of the profile $\zeta(x) = a_b\cos(2\pi x)$ for the bottom topography. We point out that the effect of bottom topography is represented by the second term in the expression for $\overline{Q}_s$ and it can thus be seen to act in a way so as to reduce the mean flow rate of the steady flow over both permeable and impermeable surfaces. Now, it has been shown experimentally by Wierschem et al. (2005) and theoretically by D'Alessio et al. (2009) that for negligible surface tension bottom topography stabilizes the flow; therefore we can associate a reduction in the mean flow rate with a more stable steady flow. Turning next to the effect of bottom permeability, we consider the quantity $\Delta\overline{Q}_s = \overline{Q}_s(\delta_1) - \overline{Q}_s(0)$ which gives the mean flow rate difference between steady flows over permeable and impermeable surfaces. We find that $\Delta\overline{Q}_s \approx 3\pi^2 a_b^2\delta_1\delta^2$ which demonstrates that bottom permeability increases the mean flow rate of the steady flow and consequently renders it more unstable.

In the next section we determine if nonlinear effects have any significant impact on the predictions presented here.

4. Nonlinear stability analysis

A stability analysis that takes into account the nonlinear effects can be carried out by examining the evolution of the perturbed equilibrium flow obtained by numerically solving the fully nonlinear governing Eqs. (8) and (9). Such a nonlinear stability analysis of gravity-driven flows has been implemented by several researchers including Kranenburg (1992), Brook et al. (1999), Chang et al. (2000), Zanuttigh and Lamberti (2002), Balmforth and Mandre (2004), Pascal and D'Alessio (2007), and D'Alessio et al. (2009).

In order to apply our numerical method we must reformulate Eq. (9) in order to express it in the form

$$\frac{\partial q}{\partial t} + \frac{\partial}{\partial x}f(h,q) = \Psi(h,q,x) + \chi\left(h, q, \frac{\partial h}{\partial x}, \frac{\partial^2 h}{\partial x^2}, \frac{\partial^3 h}{\partial x^3}, \frac{\partial q}{\partial x}, \frac{\partial^2 q}{\partial x^2}, x\right), \tag{14}$$

where the gradient of the flux function f contains terms expressed as total derivatives with respect to x. Here, Ψ denotes the terms that

do not contain the derivatives of h and q, and χ denotes the remaining derivative terms. The explicit formulation of f, Ψ and χ are discussed and given in Appendix B.

Eqs. (8) and (14) can be regarded as a system of nonlinear hyperbolic conservation laws with source terms. To deal with the derivative dependent source terms in Eq. (14) we resort to a fractional-step splitting approach. In particular, in advancing the approximate solution from one time level to the next we first consider the reduced system

$$\frac{\partial h}{\partial t}+\frac{\partial q}{\partial x}=0,$$
$$\frac{\partial q}{\partial t}+\frac{\partial}{\partial x}f(h,q)=\Psi(h,q,x).$$

This system can be effectively dealt with by the scheme proposed by Bale et al. (2003). This method is a modification of the high-resolution wave-propagation algorithm first introduced by Leveque (1997) and involves utilizing an eigenvector decomposition of flux differences instead of state variable differences. It captures the balance between the source term and the flux gradient which is appropriate for cases when the solution grows slowly in time.

In the second step of the procedure we consolidate the various derivative dependent source terms into one term denoted by χ to obtain a corrected approximation for q by solving

$$\frac{\partial q}{\partial t}=\chi\left(h,q,\frac{\partial h}{\partial x},\frac{\partial^2 h}{\partial x^2},\frac{\partial^3 h}{\partial x^3},\frac{\partial q}{\partial x},\frac{\partial^2 q}{\partial x^2},x\right). \tag{15}$$

We use the solution from the first step to set up h and its derivatives and as an initial distribution for q. Discretizing Eq. (15) by means of the Crank–Nicolson scheme and imposing periodicity conditions leads to a nonlinear system of algebraic equations which we solve iteratively using a robust algorithm which takes advantage of the structure and sparseness of the resulting linearized system.

We can use our numerical method to calculate the temporal evolution of a certain initial flow over a periodic spatial domain the length of which is arbitrary but equal to a whole multiple of the scaled wavelength of the bottom undulations. As an initial flow for our calculations we use the approximate solution to our steady-state problem. The error associated with the approximation serves as a small-amplitude wide-band perturbation, and the evolution of the perturbed state reveals the instability of the flow under consideration. For a fixed computational domain we can consider various flow conditions and thus determine the critical values of the flow parameters for instability. Since the assumed computational domain length places an upper bound on the wavelength of the included perturbation components, we can conclude that only components with wavenumber $K \leqslant 2\pi/L$, with L being the length of the computational domain, are unstable under these conditions. These results can be compared with the predictions from the linear analysis, and for the cases that were considered good agreement was found between the two, as illustrated in Fig. 9.

A comparison of our predictions of the critical conditions for flow instability with experimental data can serve as a check of the validity of the approximations associated with our depth-integrated model. Such experimental data is not available for flows over porous substrates, however an experimental verification of our results is possible for the impermeable bottom case.

Liu et al. (1993) have carried out experiments on the flow along an even impermeable surface of a glycerine–water film with parameters: $\theta = 5.6^\circ, \nu = 5.02\times10^{-6}m^2/s$ (kinematic viscosity), $\rho = 1.13\times10^3 kg/m^3$ and $T = 6.9\times10^{-2}N/m$ (surface tension). The fluid properties correspond to a Kapitza number of $Ka = 331.85$, with this nondimensional number being defined as $Ka = T/(\rho g^{1/3}\nu^{4/3})$ and related to the our parameter S by $S = (3/\sin\theta)^{1/3}Ka/\mathrm{Re}^{5/3}$. For various Reynolds numbers Liu et al. report the critical frequency, f, for

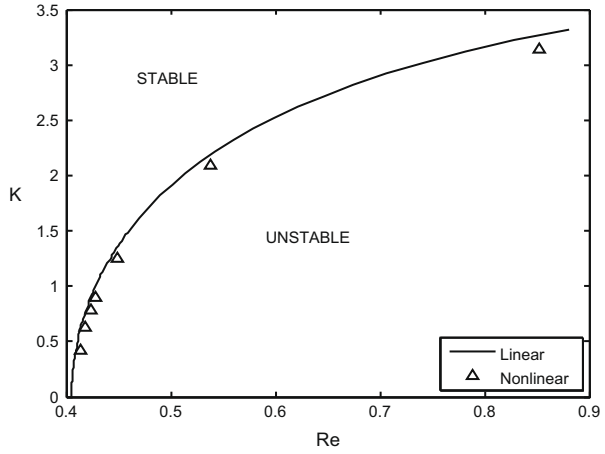

Fig. 9. Neutral stability curve for $S = 10$, $\delta_1 = 0.1$, $a_b = 0.1$, $\delta = 0.1$ and $\cot\theta = 0.5$.

perturbations to become unstable. This dimensional frequency is related to our nondimensional wavenumber, k, through the expression

$$k\delta = \left(\frac{3}{g\sin\theta}\right)^{2/3}\frac{2\pi\nu^{1/3}f}{c\mathrm{Re}^{1/3}},$$

where $c = 3$ is the dimensionless phase speed and f is in Hz. From our linear stability analysis we obtain the following relationship for neutral stability for flow over an even impermeable surface

$$\frac{5}{6}\frac{\cot\theta}{\mathrm{Re}} = \frac{175+5(k\delta)^2-33(k\delta)^4}{7[5+9(k\delta)^2]^2}-\frac{5}{18}S(k\delta)^2. \tag{16}$$

In Fig. 10 we present this relationship in the $\mathrm{Re}-k\delta$ plane together with the experimental data. The agreement is quite reasonable given that the Reynolds numbers under consideration range approximately from 8.5 to 16 and our model is only of second-order in δ if $\mathrm{Re} = O(1)$.

For the case of flow along an impermeable uneven bottom, we can compare our results for the critical Reynolds number for the onset of instability with those from the experimental work of Wierschem et al. (2005). Their setup consisted of a wavy bottom with three equal sinusoidal corrugations with a ratio of amplitude to wavelength given by

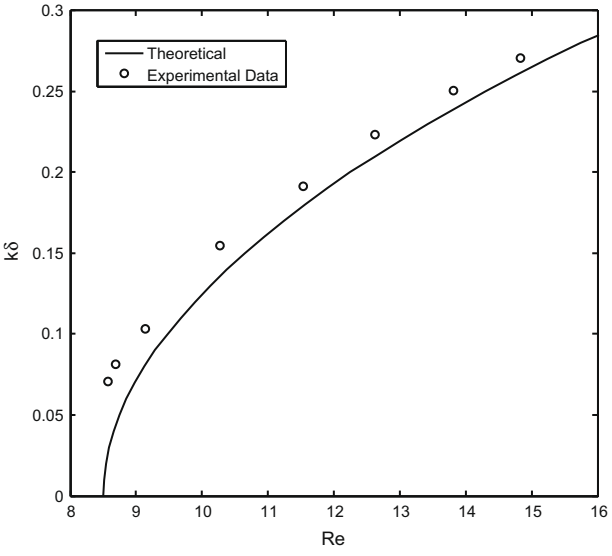

Fig. 10. Comparison between experimental and theoretical neutral stability curves for the even impermeable bottom case with $\theta = 5.6^\circ$ and $Ka = 331.85$.

Table 1
Comparison with experimental results for Re_{crit} for the impermeable case with $a_b = 0.5$ and $\delta = 0.1$.

θ (°)	Re_{crit}		
	Experimental	Nonlinear simulations	Linear stability analysis
15	5.1 ± 0.4	(5.5, 5.6)	5.6
30	2.2 ± 0.2	(1.8, 1.9)	1.7
40.7	1.3 ± 0.1	(1.1, 1.2)	1.1

$A_b/\lambda_b = 0.05$. The fluid layer was a silicone oil (B200) with $\nu = 2.24 \times 10^{-4}$ m^2/s, $\rho = 9.68 \times 10^2$ kg/m^3 and $T = 2.07 \times 10^{-2}$ N/m. Table 1 indicates good agreement between the experimental data and the predictions from our model. Our results were obtained with $a_b = 0.5$ and $\delta = 0.1$, and the experimental data is expressed in terms of our definition of the Reynolds number.

It should be pointed out that comparisons of our results with the experimental observations of Vlachogiannis and Bontozoglou (2002) are not appropriate since the wavy bottom used in that study consists of a square wave instead of a sinusoidal wave which we consider here. The square wave can be thought of as a Fourier series of harmonics of the fundamental wavelength which will interact and consequently affect the stability characteristics.

We next focus on following the development of the unstable flow and determining the final wave structure which describes the secondary flow arising from the instability. We chose to present the variation of q with x as opposed to that of h since the latter more noticeably exhibits the short-scale variations induced by the bottom undulations, and as a result small amplitude deviations from the equilibrium solution are less evident. The evolution illustrated in Fig. 11 resembles that observed in film flows along even and impermeable surfaces as noted in Chang (1994). In particular, q as a function of x, which is initially uniform, becomes sinusoidal with the amplitude growing in time. The development continues and culminates in the appearance of the famed teardrop-shaped solitary waves. Subsequently, the growth of the deflection from equilibrium saturates and the waveform becomes permanent.

In Fig. 12 we display some permanent solutions for q corresponding to different Re values. It can be seen that with $Re = 1$ the small amplitude sinusoidal wave pattern that appears in the early stages of the development of the unstable flow persists and does not evolve into the solitary waveforms seen for the larger Re values. We have also found the sinusoidal wave pattern for $Re = 1$ to remain permanent on larger computational domains. It turns out that for the parameter values considered in Fig. 12 $Re_{crit} \approx 0.81$ and it is thus apparent that with $Re = 1$ the instability

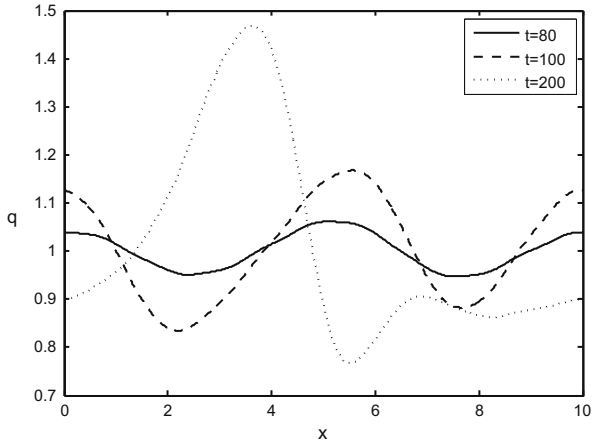

Fig. 11. The evolution of q as a function of x with $\cot\theta = 1$, $a_b = 0.15$, $\delta_1 = 0.1$, $\delta = 0.1$, $S = 100$ and $Re = 2$.

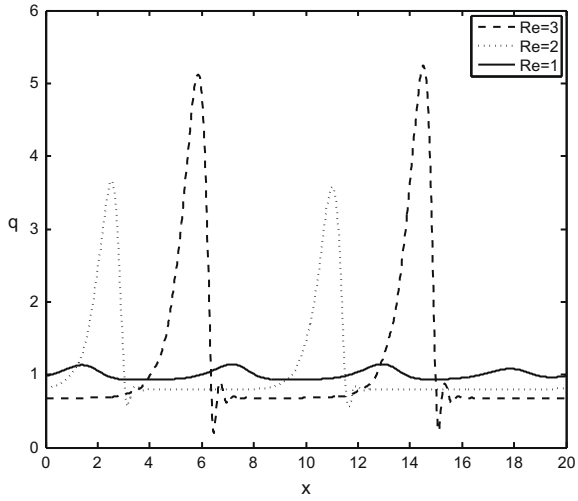

Fig. 12. The permanent solution for q as a function of x with $\cot\theta = 1$, $a_b = 0.15$, $\delta_1 = 0.1$, $\delta = 0.1$ and $S = 10$.

is not sufficiently strong to generate the growth in wave amplitude necessary for the formation of solitary waves. In Fig. 13 we present the free-surface profiles corresponding to the case considered in Fig. 12. The profile for $Re = 3$ is not included so as not to clutter the figure, but it was found to have a larger amplitude than that for $Re = 2$, and we thus conclude that the amplitude of interfacial waves increases as flow conditions become more unstable.

5. Concluding remarks

In this investigation we have developed and implemented a model for gravity-driven free-surface flow over a permeable incline with periodic undulations. A linear stability analysis was performed to determine the critical conditions for the instability of the steady flow. Several nonlinear simulations of the evolution of perturbed steady flows were conducted which confirmed the onset of instability as predicted by the linear analysis.

When interpreting the results, particular attention was focused on whether bottom topography acts to stabilize or destabilize the flow. The indication is that the destabilizing role of bottom topography is strongly dependent on the surface tension of the fluid layer, the inclination of the bottom surface and the wavelength

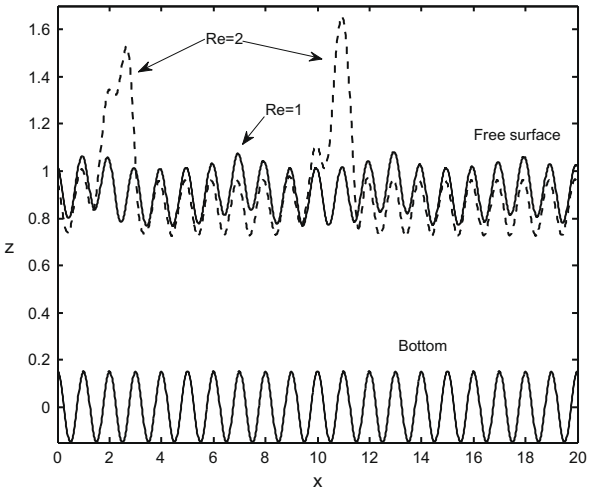

Fig. 13. The permanent free-surface profile with $\cot\theta = 1$, $a_b = 0.15$, $\delta_1 = 0.1$, $\delta = 0.1$ and $S = 10$.

of the undulations that generate the bottom topography. Our investigation reveals that in spite of being restricted to small values by the assumptions of our model, in certain cases, bottom permeability has an important impact on the instability of the flow. We found that for particular values of the surface tension parameter and δ (the scaled wavenumber of the bottom undulations) introducing bottom permeability reverses the stabilizing effect of topography. This investigation found that in general bottom permeability destabilizes the flow since it was found to alter the steady-state flow in such a way so as to render it more unstable.

Acknowledgments

Financial support for this research was provided by the Natural Sciences and Engineering Research Council of Canada. The authors gratefully acknowledge Prof. Nuri Aksel for providing us with experimental data and helpful discussions.

Appendix A. The first-order Benney equation

Another technique of determining the instability threshold involves deriving the Benney equation. This equation describes the evolution of the free surface and for the problem considered in this investigation we must first expand u, w and p in powers of δ as follows:

$$u = u_0 + \delta u_1 + \cdots,$$
$$w = w_0 + \delta w_1 + \cdots,$$
$$p = p_0 + \delta p_1 + \cdots.$$

Substituting these into the continuity and momentum equations, which to first-order become

$$\frac{\partial u}{\partial x} + \frac{\partial w}{\partial z} = 0, \tag{A1}$$

$$\delta \mathrm{Re}\left(\frac{\partial u}{\partial t} + u\frac{\partial u}{\partial x} + w\frac{\partial u}{\partial z}\right) = -\delta \mathrm{Re}\frac{\partial p}{\partial x} + 3 + \frac{\partial^2 u}{\partial z^2}, \tag{A2}$$

$$0 = -\mathrm{Re}\frac{\partial p}{\partial z} - 3\cot\theta + \delta\frac{\partial^2 w}{\partial z^2}, \tag{A3}$$

then leads to a hierarchy of problems. For orders $n = 0, 1$ the quantities u_n, w_n and p_n can be found by applying the boundary conditions, which to first-order are

$$w = \zeta' u,\ \delta_1\frac{\partial u}{\partial z} = u \text{ at } z = \zeta,$$
$$p = \frac{2\delta}{\mathrm{Re}}\frac{\partial w}{\partial z},\ \frac{\partial u}{\partial z} = 0 \text{ along } z = z_1.$$

Evaluating these expressions along the free surface $z = z_1$ and inserting them into the kinematic condition yields to first-order

$$\frac{\partial h}{\partial t} + u_0(z_1)\left(\frac{\partial h}{\partial x} + \zeta'\right) - w_0(z_1) + \delta\left[u_1(z_1)\left(\frac{\partial h}{\partial x} + \zeta'\right) - w_1(z_1)\right] = 0.$$

Determining u_n, w_n, p_n for $n = 0, 1$ is a straight-forward, albeit tedious, task. Since little is gained in the details, we omit the algebra and move directly to the final result for the first-order Benney equation for an uneven bottom

$$\frac{\partial h}{\partial t} + \frac{\partial}{\partial x}\left(h^3 + 3\delta_1 h^2\right) + \delta\frac{\partial}{\partial x}\left[\frac{6\mathrm{Re}}{5}h^6\frac{\partial h}{\partial x} + \frac{36\delta_1\mathrm{Re}}{5}h^5\frac{\partial h}{\partial x} + 15\delta_1^2\mathrm{Re}h^4\frac{\partial h}{\partial x} - \cot\theta h^3\left(\frac{\partial h}{\partial x} + \zeta'\right) - 3\delta_1\cot\theta h^2\left(\frac{\partial h}{\partial x} + \zeta'\right)\right] = 0. \tag{A4}$$

We next linearize (A4) using $h = h_0 + \hat{h}$ with $h_0 = 1 - \delta_1 + \delta_1^2 + O(\delta_1^3)$ and introduce the perturbation $\hat{h} = \tilde{h}e^{ikx}e^{\sigma t}$. For an even bottom $\zeta = 0$ and it easily follows that the instability threshold becomes

$$\mathrm{Re}_{crit}^{even} = \frac{5}{6}\cot\theta\left(1 - \frac{7}{2}\delta_1^2\right) + O(\delta_1^3). \tag{A5}$$

Although this result is not in exact agreement with that obtained from the modified IBL model presented in Section 3, the difference is of $O(\delta_1^2)$. Since our modified IBL model was derived based on the assumption that $\delta_1 = O(\delta)$, the difference between the two results is of $O(\delta^2)$. Thus, the second-order difference between the two results for $\mathrm{Re}_{crit}^{even}$ is due to the fact that the Benney equation is only first-order in δ.

Appendix B. Reformulation of the governing equations

In this appendix we discuss the reformulation of Eq. (9) in the form of Eq. (14). We point out that this formulation is not unique and that it is not possible to have all first-order derivative terms included in the gradient of f. For the original IBL equations all the first-order derivative terms arising from the advective terms of the equations of motion can be included in the gradient of the flux function, and appear in f as the term $\frac{6}{5}\frac{q^2}{h}$. Julien and Hartley (1986) used this form of the IBL equations to theoretically calculate the celerity of roll waves and showed that the results are in good agreement with their experimental observations. For the modified IBL equations a similar term can be incorporated into the flux function, however certain quasilinear derivative terms must be included as a source term. When reformulating Eq. (9), a consideration worth keeping in mind is to construct it in such a way so that when $\delta_1 = 0$ we recover the formulation for the impermeable case as proposed by D'Alessio et al. (2009). This is beneficial since permeability effects are not expected to alter the results in a significant way. One such formulation consists of Eq. (14) with

$$f = \frac{9}{7}\frac{q^2}{h} + \frac{5\cot\theta}{4\mathrm{Re}}\left(h^2 + 2\delta_1 h\right), \tag{B1}$$

$$\chi = F_1 q\frac{\partial q}{\partial x} - \frac{18\delta_1}{7}\frac{q^2}{hF}\frac{\partial h}{\partial x} + \frac{5\delta^2 SF_2h^2}{6F}\frac{\partial^3 h}{\partial x^3} + \frac{\delta}{\mathrm{Re}F}\left[\frac{9}{2}h^2\frac{\partial^2 q}{\partial x^2} - \frac{9}{2}h\frac{\partial q}{\partial x}\frac{\partial h}{\partial x} - 6qh\frac{\partial^2 h}{\partial x^2} + 4q\left(\frac{\partial h}{\partial x}\right)^2 - \frac{5}{2}\zeta' q\frac{\partial h}{\partial x}\right], \tag{B2}$$

$$\Psi = -\frac{45}{16}\frac{\delta_1\zeta'}{hF}q^2 + \frac{5}{2\delta\mathrm{Re}}\left(\frac{F_2h^2 - q}{F}\right) - \frac{5\cot\theta}{2\mathrm{Re}}\frac{F_2h^2\zeta'}{F} + \frac{5\delta^2 SF_2h^2}{6F}\zeta''' + \frac{\delta}{\mathrm{Re}F}\left(-\frac{15}{4}\zeta'' qh - 5(\zeta')^2 q\right),$$

where

$$F(\delta_1, h) = h^2 + 2\delta_1 h,\ F_1(\delta_1, h) = \frac{h + 19\delta_1}{7F} \text{ and } F_2(\delta_1, h) = h + 3\delta_1.$$

The first two terms in the expression for χ are advective terms not included in the flux function. Another possibility is to cast the governing equations in the form of Eq. (14) with

$$f = \left(\frac{9}{7} + \delta_1\right)\frac{q^2}{h} + \frac{5\cot\theta}{4\mathrm{Re}}(h^2 + 2\delta_1 h), \tag{B3}$$

and

$$\chi = \left(F_1 + \frac{2\delta_1}{h}\right)q\frac{\partial q}{\partial x} - \left(\frac{1}{h^2} + \frac{18}{7hF}\right)\delta_1 q^2\frac{\partial h}{\partial x} + \frac{5\delta^2 SF_2h^2}{6F}\frac{\partial^3 h}{\partial x^3} + \frac{\delta}{\mathrm{Re}F}\left[\frac{9}{2}h^2\frac{\partial^2 q}{\partial x^2} - \frac{9}{2}h\frac{\partial q}{\partial x}\frac{\partial h}{\partial x} - 6qh\frac{\partial^2 h}{\partial x^2} + 4q\left(\frac{\partial h}{\partial x}\right)^2 - \frac{5}{2}\zeta' q\frac{\partial h}{\partial x}\right], \tag{B4}$$

where the advective terms not included in the flux function are the first two terms in the expression for χ.

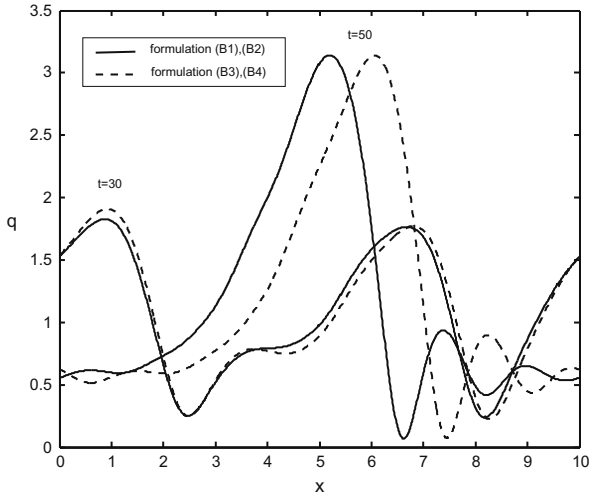

Fig. 14. The evolution of q as a function of x for $\cot\theta = 1,\ a_b = 0.15,\ \delta_1 = 0.5,\ \delta = 0.1,\ S = 100$ and $\mathrm{Re} = 3.5$.

The results in Figs. 11–13 were obtained using f and χ given by equations (B1) and (B2). In Fig. 14 we present results for q as a function of x comparing the results from the two formulations (B1),(B2) and (B3), (B4). In this example we used an extreme value of δ_1 so as to accentuate the difference. It can be seen that the structure of the solution is the same with only a small difference in the speed of propagation of the solitary wave. Indeed, we found the two formulations to give identical predictions for the critical conditions for instability.

Appendix C. Supplementary material

Supplementary data associated with this article can be found, in the online version, at doi:10.1016/j.ijmultiphaseflow.2010.03.003.

References

Bale, D.S., Leveque, R.J., Mitran, S., Rossmanith, J.A., 2003. A wave propagation method for conservation laws and balance laws with spatially varying flux functions. SIAM J. Sci. Comput. 24, 955–978.

Balmforth, N.J., Mandre, S., 2004. Dynamics of roll waves. J. Fluid Mech. 514, 1–33.

Beavers, G.S., Joseph, D.D., 1967. Boundary conditions at a naturally permeable wall. J. Fluid Mech. 30, 197–207.

Benjamin, T.B., 1957. Wave formation in laminar flow down an inclined plane. J. Fluid Mech. 2, 554–574.

Benney, D.J., 1966. Long waves on liquid films. J. Maths Phys. 54, 150–155.

Bontozoglou, V., Papapolymerou, G., 1997. Laminar film flow down a wavy incline. Int. J. Multiphase Flow 1, 69–79.

Brook, B.S., Pedley, T.J., Falle, S.A., 1999. Numerical solutions for unsteadygravity-driven flows in collapsible tubes: evolution and roll-wave instability of a steady state. J. Fluid Mech. 396, 223–256.

Chang, H.-C., 1994. Wave evolution on a falling film. Annu. Rev. Fluid Mech. 26, 103–136.

Chang, H.-C., Demekhin, E.A., Kalaidin, E., 2000. Coherent structures, self-similarity and universal roll wave coarsening dynamics. Phys. Fluids 12, 2268–2278.

Chang, M., Chen, F., Straughan, B., 2006. Instability of Poiseuille flow in a fluid overlying a porous layer. J. Fluid Mech. 564, 287–303.

Craster, R.V., Matar, O.K., 2009. Dynamics and stability of thin liquid films. Rev. Mod. Phys. 81, 1131–1198.

D'Alessio, S.J.D., Pascal, J.P., Jasmine, H.A., 2009. Instability in gravity-driven flow over uneven surfaces. Phys. Fluids 21, 062105.

Davalos-Orozco, L.A., 2007. Nonlinear instability of a thin film flowing down a smoothly deformed surface. Phys. Fluids 19, 074103.

Davis, S.H., Hocking, L.M., 1999. Spreading and imbibition of viscous liquid on a porous base. Phys. Fluids 11, 48–57.

Heining, C., Aksel, N., 2009. Bottom reconstruction in thin-film flow over topography: steady solution and linear stability. Phys. Fluids 21, 083605.

Heining, C., Bontozoglou, V., Aksel, N., Wierschem, A., 2009. Nonlinear resonance in viscous films on inclined wavy planes. Int. J. Multiphase Flow 35, 78–90.

Jones, I.P., 1973. Low Reynolds number flow past a porous spherical shell. Proc. Camb. Phil. Soc. 73, 231–238.

Julien, P., Hartley, D., 1986. Formation of roll waves in laminar sheet flow. J. Hydraul. Res. 24, 5–17.

Kranenburg, C., 1992. On the evolution of roll waves. J. Fluid Mech. 245, 249–261.

Leveque, R.J., 1997. Wave propagation algorithms for multi-dimensional hyperbolic systems. J. Comput. Phys. 131, 327–335.

Liu, J., Paul, J.D., Gollub, J.P., 1993. Measurements of the primary instabilities of film flows. J. Fluid Mech. 250, 69–101.

Liu, J., Schneider, B., Gollub, J.P., 1995. Three-dimensional instabilities of film flows. Phys. Fluids 7, 55–67.

Liu, R., Liu, Q.S., Zhao, S.C., 2008. Instability of plane Poiseuille flow in a fluid–porous system. Phys. Fluids 20, 104105.

Malamataris, N.A., Vlachogiannis, M., Bontozoglou, V., 2002. Solitary waves on inclined films: flow structure and binary interactions. Phys. Fluids 14, 1082–1094.

Miglio, E., Quarteroni, A., Saleri, F., 2003. Coupling of free surface and groundwater flows. Comput. Fluids 32, 73–83.

Needham, D., Merkin, J., 1984. On roll waves down an open inclined channel. Proc. Roy. Soc. Lond. A 394, 259–278.

Oron, A., Heining, C., 2008. Weighted-residual integral boundary-layer model for the nonlinear dynamics of thin liquid films falling on an undulating vertical wall. Phys. Fluids 20, 082102.

Pascal, J.P., 1999. Linear stability of fluid flow down a porous inclined plane. J. Phys. D 32, 417–422.

Pascal, J.P., 2006. Instability of power-law fluid flow down a porous incline. J. Non-Newtonian Fluid Mech. 133, 109–120.

Pascal, J.P., D'Alessio, S.J.D., 2007. Instability of power-law fluid flows down an incline subjected to wind stress. Appl. Math. Modell. 31, 1229–1248.

Pozrikidis, C., 1988. The flow of a liquid film along a periodic wall. J. Fluid Mech. 188, 275–300.

Ramaswamy, B., Chippada, S., Joo, S.W., 1996. A full-scale numerical study of interfacial instabilities in thin-film flows. J. Fluid Mech. 325, 163–194.

Ruyer-Quil, C., Manneville, P., 2000. Improved modeling of flows down inclined planes. Eur. Phys. J.B 15, 357–369.

Ruyer-Quil, C., Manneville, P., 2002. Further accuracy and convergence results on the modeling of flows down inclined planes by weighted-residual approximations. Phys. Fluids 14, 170–183.

Sadiq, I.M.R., Usha, R., 2008. Thin Newtonian film flow down a porous inclined plane: stability analysis. Phys. Fluids 20, 022105.

Saffman, P., 1971. On the boundary conditions at the surface of a porous medium. Stud. Appl. Maths 50, 93–101.

Scheid, B., Ruyer-Quil, C., Manneville, P., 2006. Wave patterns in film flows: modelling and three-dimensional waves. J. Fluid Mech. 562, 183–222.

Shkadov, V.Y., 1967. Wave conditions in flow of thin layer of a viscous liquid under the action of gravity. Izv. Akad. Nauk SSSR, Mekh. Zhidh. Gaza 1, 43–50.

Thiele, U., Goyeau, B., Velarde, M., 2009. Stability analysis of thin film flow along a heated porous wall. Phys. Fluids 21, 014103.

Tougou, H., 1978. Long waves on a film flow of a viscous fluid down an inclined uneven wall. J. Phys. Soc. Jpn. 44, 1014–1019.

Trifonov, Y.Y., 1998. Viscous liquid film flows over a periodic surface. Int. J. Multiphase Flow 24, 1139–1161.

Trifonov, Y.Y., 2007a. Stability and nonlinear wavy regimes in downward film flows on a corrugated surface. J. Appl. Mech. Tech. Phys. 48, 91–100.

Trifonov, Y.Y., 2007b. Stability of a viscous liquid film flowing down a periodic surface. Int. J. Multiphase Flow 33, 1186–1204.

Vlachogiannis, M., Bontozoglou, V., 2002. Experiments on laminar film flow along a periodic wall. J. Fluid Mech. 457, 133–156.

Wang, C.Y., 1981. Liquid film flowing slowly down a wavy incline. AIChE J. 27, 207–212.

Wierschem, A., Lepski, C., Aksel, N., 2005. Effect of long undulated bottoms on thin gravity-driven films. Acta Mech. 179, 41–66.

Yih, C.-S., 1963. Stability of liquid flow down an inclined plane. Phys. Fluids 6, 321–334.

Zanuttigh, B., Lamberti, A., 2002. Roll waves simulation using shallow water equations and weighted average flux method, J. Hydraul. Res. 553, 610–622.